J. Fluid Mech. (2017), *vol.* 829, *pp.* 112–126. © Cambridge University Press 2017
doi:10.1017/jfm.2017.557

Algebraic disturbance growth by interaction of Orr and lift-up mechanisms

M. J. Philipp Hack[1,†] **and Parviz Moin**[1]

[1]Center for Turbulence Research, Stanford University, Stanford, CA 94305, USA

(Received 10 April 2017; revised 11 July 2017; accepted 4 August 2017;
first published online 14 September 2017)

Algebraic disturbance growth in spatially developing boundary-layer flows is investigated using an optimization approach. The methodology builds on the framework of the parabolized stability equations and avoids some of the limitations associated with adjoint-based schemes. In the Blasius boundary layer, non-parallel effects are shown to significantly enhance the energy gain due to algebraic growth mechanisms. In contrast to parallel flow, the most energetic perturbations have finite frequency and are generated by the simultaneous activity of the Orr and lift-up mechanisms. The highest amplification occurs in a limited region of the parameter space that is characterized by a linear relation between the wavenumber and frequency of the disturbances. The frequency of the most highly amplified perturbations decreases with Reynolds number. Adverse streamwise pressure gradient further enhances the amplification of disturbances while preserving the linear trend between the wavenumber and frequency of the most energetic perturbations.

Key words: boundary layers, boundary layer stability

1. Introduction

In shear flows exposed to sources of excitation such as external perturbations, the exponential amplification of disturbances is often outpaced by algebraic, or non-modal, amplification mechanisms. The prevalent outcome of algebraic growth in zero-pressure-gradient (ZPG) boundary layers are streamwise elongated streaks which are highly energetic perturbations in the streamwise velocity component that can lead to fast breakdown to turbulence via the growth of high-frequency secondary instabilities. This work examines the conditions which lead to algebraic disturbance growth in non-parallel boundary layers using an optimization approach within the framework of the parabolized stability equations.

Algebraic energy growth is independent of the exponential stability of the flow and as such eludes a characterization based on the eigenvalues of the linear operator. In formal terms, algebraic growth mechanisms can be ascribed to the non-orthogonal nature of the eigenfunctions of the linearized governing equations. Even when all modes are exponentially stable, their varying decay rates can enable a temporary gain in the kinetic energy of disturbances (Trefethen *et al.* 1993). This transient nature

† Email address for correspondence: mjph@stanford.edu

of algebraic mechanisms implies that there exists an upper bound for the resulting amplification of perturbation energy, and explains why laminar–turbulent transition due to the algebraic growth of primary perturbations requires conditions that provide an initial seeding of sufficient energy (Reddy & Henningson 1993).

In Blasius boundary layers, non-modal amplification of perturbations can occur via the lift-up and Orr mechanisms. The former describes the displacement of the mean momentum of the boundary layer through small disturbances in the normal velocity (Landahl 1975, 1980). One of the first parametric studies of the lift-up mechanism was conducted by Butler & Farrell (1992) who solved an optimization problem in terms of the perturbation kinetic energy. They showed that under the assumption of wall-parallel flow, the magnitude of the perturbation energy gain is highest for perturbations with zero streamwise wavenumber. The later work by Andersson, Berggren & Henningson (1999) demonstrated that the energy growth of the streaks scales linearly with the distance to the leading edge. In the ZPG boundary layer, the optimal initial condition which yields the most energetic streaks is a pair of counter-rotating, streamwise oriented vortices (see also Luchini 2000).

The mechanism identified by and named after Orr (1907) describes a second pathway for non-modal perturbation growth. The Orr mechanism amplifies disturbances whose streamlines are tilted against the mean shear and which intensify as they are reoriented by the base flow (Farrell 1987). Global stability analyses by Åkervik *et al.* (2008), which resolved both the normal and streamwise dimensions within the computational domain, showed that the Orr mechanism can optimally initiate Tollmien–Schlichting waves in Blasius boundary layers. Using a similar approach, Monokrousos *et al.* (2010) studied global optimal disturbances in the Blasius boundary layer. Their results appeared to indicate that the most highly amplified elongated perturbations in non-parallel flow are generated by a combination of the Orr and lift-up mechanisms. In the context of wall-bounded turbulence, Jimenéz (2013) credited the Orr mechanism with the augmentation of normal disturbances arising from the breakdown of streaks. According to the proposed model, these disturbances close a cyclical process by amplifying algebraically and inducing the formation of new streaks.

In general, earlier investigations of non-modal growth often relied on a parallel-flow assumption within a temporal framework. The approach enables the immediate construction of the fundamental solution operator, which relates the solutions at two different time instances, after solving the stability problem. The conditions which lead to the most highly amplified perturbations are then efficiently found by singular value decomposition (SVD). In non-parallel flows, the construction of a spatial fundamental solution operator can become computationally more demanding, which has led to operator-free approaches that aim to find its primary singular values by successively integrating the forward and adjoint stability equations. The concept has been applied in global analyses (e.g. Monokrousos *et al.* 2010) as well as in time-dependent flows (e.g. Hack & Zaki 2015). For a comprehensive review of the methodology used in the analysis of non-modal amplification mechanisms, the reader is referred to Schmid (2007).

The present work aims to quantify the interaction between the two classes of algebraic growth mechanisms as well as the role of non-parallel effects in the Blasius boundary layer. In § 2, a method for computing spatial optimal disturbances within the parabolized stability equations (PSE) framework is presented. Linear results for optimal disturbances in ZPG boundary layers are provided in § 3. The effects of favourable and adverse streamwise pressure gradients are discussed in § 4, followed by concluding remarks in § 5.

2. Computation of spatial optimal disturbances

The optimization scheme developed in this work is based on the computation of the spatial evolution of small disturbances using the parabolized stability equations (Bertolotti, Herbert & Spalart 1992; Herbert 1997). The PSE are derived from the incompressible linearized Navier–Stokes equations,

$$\frac{\partial \boldsymbol{u}}{\partial t} = -\boldsymbol{U}\cdot\nabla\boldsymbol{u} - \boldsymbol{u}\cdot\nabla\boldsymbol{U} - \frac{1}{\rho}\nabla p + \frac{1}{Re}\Delta\boldsymbol{u}, \tag{2.1}$$

$$\nabla\cdot\boldsymbol{u} = 0, \tag{2.2}$$

which describe the evolution of small perturbations, $\boldsymbol{q} = (\boldsymbol{u}^{\mathrm{T}}, p)^{\mathrm{T}} = (u, v, w, p)^{\mathrm{T}}$ to the base flow $\boldsymbol{U} = (U, V, W)^{\mathrm{T}}$. The ansatz

$$\boldsymbol{q}(x, y, z, t) = \hat{\boldsymbol{q}}(x, y)\exp\left(\mathrm{i}\int_0^x \alpha(\xi)\,\mathrm{d}\xi + \mathrm{i}\beta z - \mathrm{i}\omega t\right) \tag{2.3}$$

is invoked, where $\hat{\boldsymbol{q}}$ is the complex disturbance shape function, α is a complex streamwise wavenumber, β is a real spanwise wavenumber and ω is a real temporal frequency. The ambiguity arising from the dependence of both $\hat{\boldsymbol{q}}$ and α on x is resolved by requiring that

$$\int_0^\infty \hat{\boldsymbol{q}}^{\boldsymbol{H}}\frac{\partial\hat{\boldsymbol{q}}}{\partial x}\,\mathrm{d}y = 0, \tag{2.4}$$

where superscript $\boldsymbol{H}$ denotes the conjugate transpose. The shape function $\hat{\boldsymbol{q}}(x, y)$ hence only weakly depends on the streamwise coordinate. Retaining terms up to order $O(Re^{-1})$, the governing equations take the form,

$$\boldsymbol{D}\frac{\partial\hat{\boldsymbol{q}}}{\partial x} = -\boldsymbol{A}\hat{\boldsymbol{q}} - \boldsymbol{B}\frac{\partial\hat{\boldsymbol{q}}}{\partial y} - \boldsymbol{C}\frac{\partial^2\hat{\boldsymbol{q}}}{\partial y^2}. \tag{2.5}$$

The definitions of the matrices $\boldsymbol{A}$, $\boldsymbol{B}$, $\boldsymbol{C}$ and $\boldsymbol{D}$ for a general, three-dimensional base state $\boldsymbol{U}(x, y) = (U, V, W)^{\mathrm{T}}$ are

$$\boldsymbol{A} = \begin{pmatrix} r + \dfrac{\partial U}{\partial x} & \dfrac{\partial U}{\partial y} & 0 & \mathrm{i}\alpha \\ 0 & r + \dfrac{\partial V}{\partial y} & 0 & 0 \\ \dfrac{\partial W}{\partial x} & \dfrac{\partial W}{\partial y} & r & \mathrm{i}\beta \\ \mathrm{i}\alpha & 0 & \mathrm{i}\beta & 0 \end{pmatrix}, \quad \boldsymbol{B} = \begin{pmatrix} V & 0 & 0 & 0 \\ 0 & V & 0 & 1 \\ 0 & 0 & V & 0 \\ 0 & 1 & 0 & 0 \end{pmatrix}, \tag{2.6a,b}$$

$$\boldsymbol{C} = \begin{pmatrix} -\dfrac{1}{Re} & 0 & 0 & 0 \\ 0 & -\dfrac{1}{Re} & 0 & 0 \\ 0 & 0 & -\dfrac{1}{Re} & 0 \\ 0 & 0 & 0 & 0 \end{pmatrix}, \quad \boldsymbol{D} = \begin{pmatrix} U & 0 & 0 & 0 \\ 0 & U & 0 & 0 \\ 0 & 0 & U & 0 \\ 1 & 0 & 0 & 0 \end{pmatrix}, \tag{2.6c,d}$$

with $r = -\mathrm{i}\omega + \mathrm{i}\alpha U + \mathrm{i}\beta W + (\alpha^2 + \beta^2)/Re$. In this formulation, the spatial marching scheme of the PSE has been regularized by disregarding the term $\partial\hat{p}/\partial x$ while

maintaining the rapid change of the pressure associated with the harmonic oscillation and the exponential growth of instabilities (see Haj-Hariri 1994; Li & Malik 1996). The PSE (2.5) are discretized in the wall-normal dimension using a spectral method based on 80 Chebyshev polynomials. The marching of the equations in x is facilitated through an implicit second-order scheme with the exception of the first point, where a first-order scheme is employed. Taken as a whole, the marching procedure asymptotically attains second-order accuracy in the limit of fine grid spacing. Parameter studies showed that a streamwise resolution of 64 points was sufficient for the convergence of the results. Velocities are scaled by the free-stream value at the initial position of the streamwise marching, x_0, and lengths are normalized by the boundary-layer thickness at that location, $\delta_0 = \delta(x_0)$.

A measure of the perturbation kinetic energy at a specific streamwise position is given by the energy norm

$$\|\boldsymbol{h}\|_E^2 \equiv \int_0^\infty u^* u + v^* v + w^* w \, \mathrm{d}y, \tag{2.7}$$

where superscript $*$ denotes the complex conjugate. The objective of finding the initial solution $\boldsymbol{h}_0$ which yields the highest gain in perturbation energy between the initial position x_0 and a final position x_1 is equivalent to maximizing the functional

$$G(x_0, x_1) \equiv \max_{\boldsymbol{h}_0} \frac{\|\boldsymbol{h}_1\|_E}{\|\boldsymbol{h}_0\|_E} = \max_{\boldsymbol{h}_0} \frac{\|\boldsymbol{L}\boldsymbol{h}_0\|_E}{\|\boldsymbol{h}_0\|_E}. \tag{2.8}$$

Here, $\boldsymbol{L}$ is the spatial fundamental solution operator which advances an arbitrary perturbation field from the initial to the final position.

Reddy, Schmid & Henningson (1993) studied the temporal optimal disturbances for a parallel base state. They described the initial perturbation in terms of a weighted superposition of eigenfunctions of the temporal Orr–Sommerfeld operator. Since the problem was linear, the time evolution of the superposition was governed by the growth rates of the individual modes. A similar approach is pursued here, although in the context of a spatially developing flow. The local eigenfunctions of the spatial Orr–Sommerfeld and Squire system are evaluated at the position $x_e < x_0$ and are adopted as an initial guess for a basis to represent the disturbance field. The initial streamwise wavenumber for the marching is as well taken from the eigenvalue problem. The actual basis is obtained by individually marching the modes from x_e to x_0 using the PSE.

The absence of non-parallel effects in the Orr–Sommerfeld/Squire problem leads to a small transient when using the modes as an initial condition for the PSE marching (see e.g. Herbert 1994). This effect is visualized in figure 1(*a*) which shows the real part of the streamwise wavenumber of a single mode as a function of the streamwise coordinate. A comparison of the original eigenfunction at x_e and the marched PSE solution at x_0 is provided in figure 1(*b*) and shows that the two solutions are virtually identical.

The computational effort of the optimization procedure is reduced by exploiting the rapid convergence of G under an expansion of the optimal disturbance, $\boldsymbol{h}_0$, in terms of eigenfunctions of the spatial Orr–Sommerfeld problem. The underlying rationale is that the most stable modes decay so quickly that they are in essence irrelevant to the transient amplification of disturbances (see e.g. Reddy & Henningson 1993). Considering only the k least stable eigenfunctions, the optimal initial condition can be written as,

$$\boldsymbol{h}_0 = \boldsymbol{Q}_0 \boldsymbol{\kappa}. \tag{2.9}$$

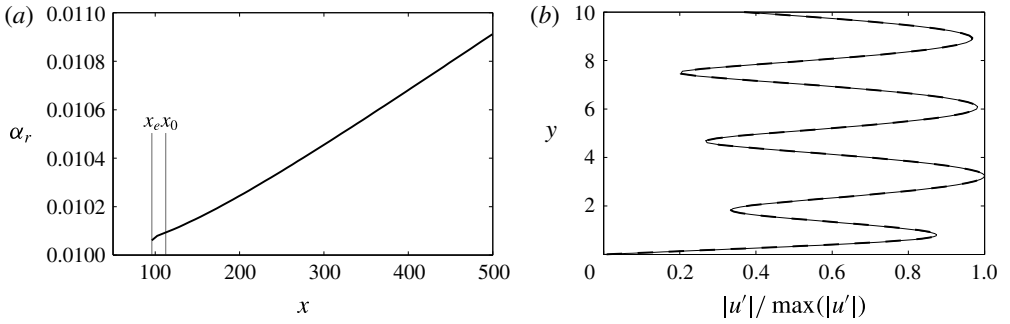

FIGURE 1. (*a*) Real part of the streamwise disturbance wavenumber of an eigenfunction with $\beta = 1.8$, $\omega = 0.01$, computed by PSE marching starting from a spatial Orr–Sommerfeld eigenfunction at x_e. (*b*) Absolute of the streamwise component of the eigenfunction computed via the solution of the eigenvalue problem at x_e (solid) and via PSE marching from x_e to x_0 (dashed).

Here, the columns of $\boldsymbol{Q}_0 \in \mathbb{C}^{4n\times k}$ are the k eigenfunctions, $\hat{\boldsymbol{q}}(x_0, y)\exp(\mathrm{i}\int_{x_e}^{x_0}\alpha(\xi)\,\mathrm{d}\xi)$, n is the number of grid points in the wall-normal dimension and $\boldsymbol{\kappa} \in \mathbb{C}^{k\times 1}$ are the weights of the individual modes. Similarly, the solution at the final position is

$$\boldsymbol{h}_1 = \boldsymbol{Q}_1\boldsymbol{\kappa}, \tag{2.10}$$

with the columns of $\boldsymbol{Q}_1$ representing the solutions obtained from evolving the k eigenfunctions in $\boldsymbol{Q}_0$ from x_0 to x_1. Since the geometric multiplicity of the eigenfunctions of the Orr–Sommerfeld/Squire system is one, the operator $\boldsymbol{Q}_0$ has full column rank, $\mathrm{rk}\,\boldsymbol{Q}_0 = k\ \forall\ k \in [1, 4n]$, and $\boldsymbol{Q}_0^{\boldsymbol{H}}\boldsymbol{Q}_0$ is invertible. The Moore–Penrose pseudo-inverse of $\boldsymbol{Q}_0$ is hence explicitly defined as

$$\boldsymbol{Q}_0^{+} \equiv (\boldsymbol{Q}_0^{\boldsymbol{H}}\boldsymbol{Q}_0)^{-1}\boldsymbol{Q}_0^{\boldsymbol{H}}. \tag{2.11}$$

The full column rank of $\boldsymbol{Q}_0$ further implies that $\boldsymbol{Q}_0^{+}$ is a left inverse, so that $\boldsymbol{Q}_0^{+}\boldsymbol{Q}_0 \equiv \boldsymbol{I}$, and specifically,

$$\boldsymbol{h}_1 = \boldsymbol{Q}_1\boldsymbol{Q}_0^{+}\boldsymbol{h}_0. \tag{2.12}$$

The matrix $\widetilde{\boldsymbol{L}}_k \equiv \boldsymbol{Q}_1\boldsymbol{Q}_0^{+}$ thus defines an exact pseudo-fundamental solution operator which advances arbitrary superpositions of the first k eigenfunctions from x_0 to x_1. The solution to the optimization problem in terms of the k modes is therefore

$$G_k(x_0, x_1) = \max_{\boldsymbol{h}_0}\frac{\|\widetilde{\boldsymbol{L}}_k\boldsymbol{h}_0\|_E}{\|\boldsymbol{h}_0\|_E} = \max_{\boldsymbol{h}_0}\frac{\|\boldsymbol{F}\widetilde{\boldsymbol{L}}_k\boldsymbol{h}_0\|_2}{\|\boldsymbol{F}\boldsymbol{h}_0\|_2} = \|\boldsymbol{F}\widetilde{\boldsymbol{L}}_k\boldsymbol{F}^{-1}\|_2, \tag{2.13}$$

where the energy–weight matrix $\boldsymbol{F}$ is defined such that $\|\boldsymbol{F}\boldsymbol{h}\|_2 \equiv \|\boldsymbol{h}\|_E$. The 2-norm in the rightmost expression of (2.13) is equivalent to the spectral norm of $\boldsymbol{F}\widetilde{\boldsymbol{L}}_k\boldsymbol{F}^{-1}$ and is efficiently computed via singular value decomposition.

The influence of the length of the eigenfunction expansion, k, on the energy gain is visualized in figure 2. Beyond $k \gtrsim 40$, the energy amplification ratio converges increasingly to an asymptotic value of $G \approx 530$. Assuming a total of 40 modes in the optimization procedure, the computational cost is thus comparable to 20 iterations in an adjoint-based scheme.

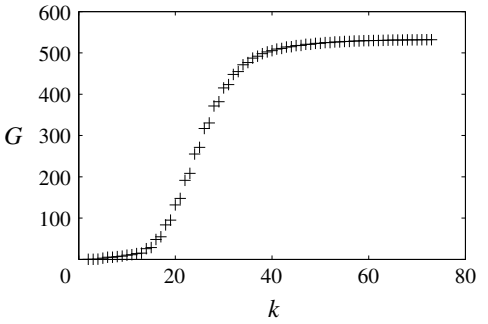

FIGURE 2. Energy amplification ratio G versus number of modes k for parameters $\omega = 10^{-6},\ \beta = 1.8,\ Re_0 = 2440$.

The above optimization scheme based on the individual spatial evolution of the constituent eigenfunctions of the optimal disturbance is suitable for two- and three-dimensional base states. It avoids some of the restrictions of adjoint-based PSE approaches which evolve the total optimal disturbance by imposing a single streamwise wavenumber (e.g. Tempelmann, Hanifi & Henningson 2010). Specifically when the optimal is described by a superposition of modes with varying streamwise wavenumber, such as eigenfunctions from both the discrete and continuous spectra, their simultaneous marching in the adjoint-based approach does not guarantee the accurate capturing of their individual evolution and by extension of the optimal disturbance as a whole (see also Towne 2016).

Furthermore, the present algorithm does not require *a priori* knowledge of the streamwise wavenumber of the optimal disturbance. Instead, its streamwise form emerges naturally from the evolution of the constituent modes. The method further allows the efficient evaluation of any $G(x_0,\ x_1')$ with $x_0 < x_1' < x_1$. Storing the intermediate spatial history of the PSE solution between x_0 and x_1 enables the immediate construction of $\widetilde{\boldsymbol{L}}_k(x_0,\ x_1')$, and the optimization problem is reduced to a re-evaluation of the SVD. This property is advantageous when the interest is in computing the globally most highly energetic perturbations for a given Reynolds number, maximized over all possible final positions.

3. Non-parallel optimal disturbances

In the following, results on the spatial growth of disturbances in non-parallel Blasius boundary layers, computed with the above described optimization framework, are presented. The first set-up considers the most highly amplified perturbations due to non-modal mechanisms for a constant initial position $x_0 = 108$, corresponding to a Reynolds number $Re = 2440$. The gain in the kinetic energy of the perturbations is maximized over all final positions,

$$G_{max} \equiv \max_{x_1} G(x_0, x_1). \tag{3.1}$$

Since the focus is on purely algebraic perturbation growth, the region of small β where an interaction of non-modal growth with the exponential Tollmien–Schlichting waves can occur (see Åkervik *et al.* 2008) is excluded from the analysis.

The maximum energy gain as a function of the disturbance frequency and the spanwise wavenumber is presented in figure 3(*a*). A band of high disturbance

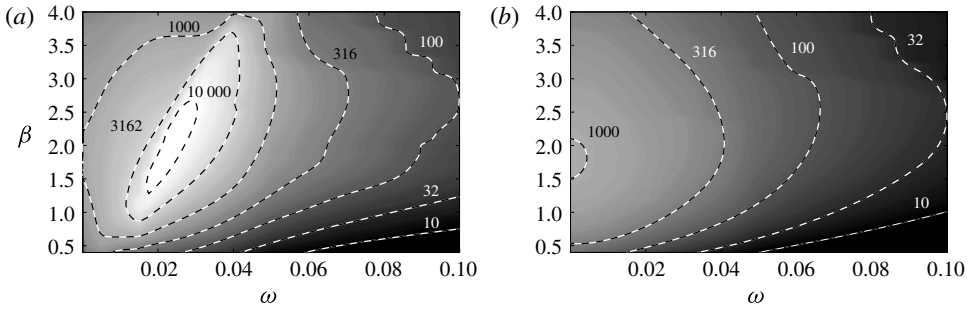

FIGURE 3. Maximum energy amplification ratio G (logarithmic scaling) at $Re_0 = 2440$ as a function of the perturbation frequency ω and the perturbation wavenumber β. (a) Non-parallel flow. (b) Parallel flow.

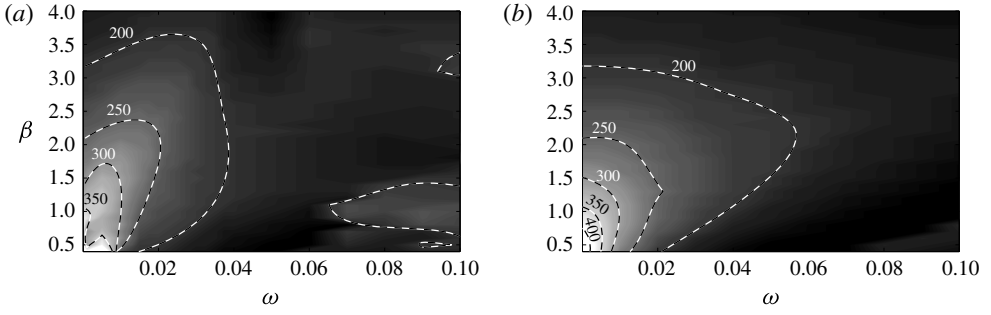

FIGURE 4. Streamwise coordinate x_1 of the highest perturbation kinetic energy at $Re_0 = 2440$ as a function of the perturbation frequency ω and the perturbation wavenumber β. (a) Non-parallel flow. (b) Parallel flow.

amplification is observed which approximately stretches from $\beta = 1.0$, $\omega = 0.013$ to $\beta = 3.5$ and $\omega = 0.040$. The global maximum of $G \approx 1.5 \times 10^4$ occurs at parameters $\beta = 1.8$ and $\omega = 0.023$. For reference, figure 3(b) shows the perturbation energy gain computed with the spatial PSE scheme, however under the assumption of a parallel base flow, i.e. by setting $U(x, y) \equiv U(x_0, y)$ and $V(x, y) \equiv 0$. The parallel results indicate a significantly lower global maximum of $G = 1031$, in line with the value of $G_t = 980$ predicted by the scaling law derived from the temporal parallel-flow analysis of Butler & Farrell (1992). In agreement with the existing literature, the most highly amplified perturbations in the parallel flow have zero frequency and a spanwise wavenumber of $\beta \approx 1.8$ based on the boundary-layer thickness at x_0. In the non-parallel case, the energy gain at these parameter is $G = 1046$, indicating that the expansion of the boundary layer has a rather limited effect on perturbations with extremely low frequency.

Contours of the streamwise location of highest perturbation kinetic energy, x_1, are provided in figure 4. The results show that the most highly energetic perturbations are observed between $x = 200$ and $x = 250$, i.e. approximately 100–150 boundary-layer thicknesses downstream of the initial position, $x_0 = 108$. The parallel-flow case presented in figure 4(b) provides a similar outcome, substantiating that non-parallel effects only marginally change the length scales of non-modal perturbation growth.

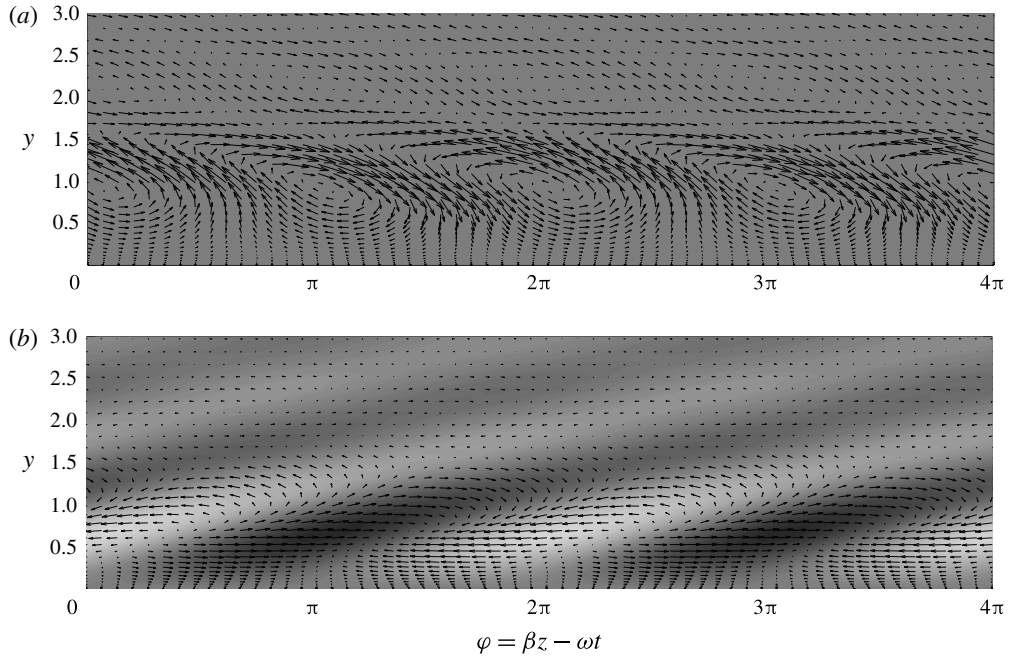

FIGURE 5. Optimal disturbance as a function of the phase $\varphi = \beta z - \omega t$. Contours of the streamwise component with vectors of the spanwise and normal components. (*a*) Initial position, $x_0 = 108$. (*b*) Position of highest kinetic energy, $x_1 = 250$.

The involvement of the Orr mechanism in the evolution of the most highly amplified disturbances becomes clear from visualizations of the solution as a function of the phase, $\varphi = \beta z - \omega t$, at the initial and final positions of the optimization scheme, see figure 5. At a location of constant spanwise coordinate z, the abscissa describes the variation of the disturbance field with time. Analogously, at a specific time instance t, the axis indicates the change of the perturbation field in the spanwise dimension. The initial field at x_0 is presented in figure 5(*a*). While the streamwise component has negligible amplitude, the spanwise and normal components form vortices which are tilted against the direction of the mean shear. At the final position (figure 5*b*), the vortices have been reoriented by the base flow. Simultaneously, the vortices have caused an amplification of the streamwise perturbation component according to the classical lift-up mechanism. The present results thus substantiate and quantify findings in global optimal growth analyses, for instance by Monokrousos *et al.* (2010), where a reorientation of perturbations that were initially tilted against the shear was reported. Their results also indicated that the most highly amplified disturbances in non-parallel flows are spatially compact and have finite length.

The total perturbation kinetic energy, $E(x) \equiv \|\boldsymbol{q}(x)\|_E$, as a function of the streamwise coordinate at parameters $\beta = 1.8$, $\omega = 0.02$ is evaluated in figure 6(*a*) for the parallel and non-parallel cases. The results show an additional energy gain of the total energy in the non-parallel flow, followed by a more rapid viscous decay than observed in the parallel case. Results for the energy in the normal and transverse components presented in figure 6(*b*) demonstrate that non-parallel effects introduce an appreciable amplification of E_w. This additional amplification of the energy in the spanwise component can be ascribed to an Orr mechanism in the cross-plane, see

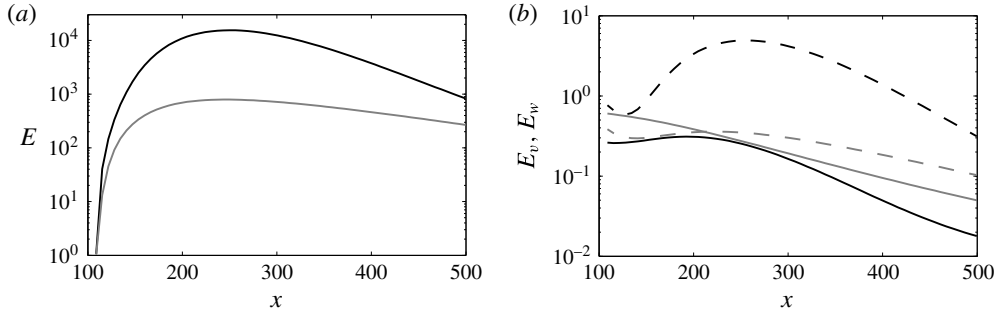

FIGURE 6. Perturbation kinetic energy as a function of streamwise coordinate at $\beta = 1.8$, $\omega = 0.02$. Non-parallel flow (black) and parallel flow (grey). (*a*) Total kinetic energy, E. (*b*) Energy in the normal component, E_v, (solid) and in the spanwise component, E_w (dashed).

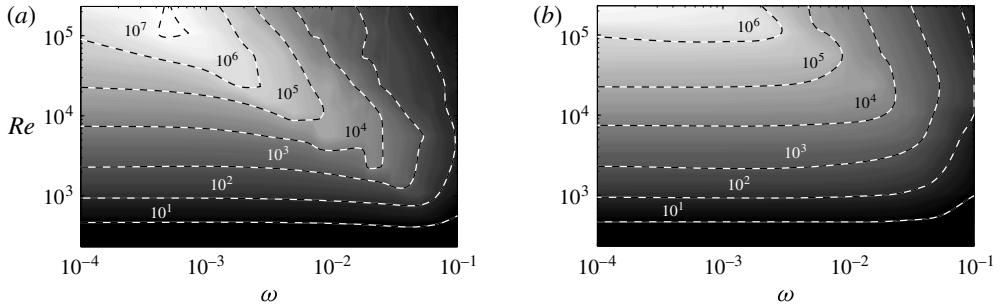

FIGURE 7. Maximum energy amplification ratio G (logarithmic scaling) at $Re_0 = 2440$ as a function of the perturbation frequency ω and the Reynolds number Re. (*a*) Non-parallel flow. (*b*) Parallel flow.

figure 5, which is augmented by the non-uniform $V(y)$ absent in parallel flow. On the other hand, the normal component remains at the same or a lower level in the non-parallel case, indicating that the additional energy gain is not due to an enhanced lift-up mechanism via stronger normal displacement of the mean momentum. We note that in both cases, the kinetic energy in the normal and spanwise perturbations remains several orders of magnitude smaller than in the streamwise perturbation component which at the peak of $E(x)$ makes up more than 99.9 % of the total kinetic energy in both the non-parallel and parallel cases.

The initial position and thus the Reynolds number of the analysis have been kept constant so far. In the remainder of this section, we aim to establish the influence of Re on algebraic growth in non-parallel boundary layers. Since algebraic growth is only limited by viscosity, the general trend of stronger growth with higher Reynolds number can also be expected to prevail in non-parallel flow. Contours of the energy amplification factor as a function of ω and Re, presented in figure 7(*a*), support this surmise. The global maximum of G within the considered parameter range is observed at the largest investigated Reynolds number, $Re = 2.2 \times 10^5$, at a finite frequency $\omega \approx 4 \times 10^{-4}$. In line with the literature on temporal optimal disturbances (e.g. Butler & Farrell 1992), the optimal frequency in the parallel case presented in figure 7(*b*) is zero for all Reynolds numbers.

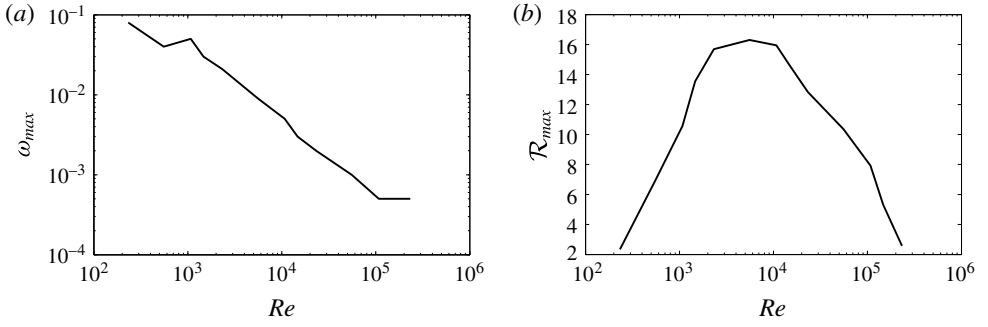

FIGURE 8. (*a*) Frequency ω_{max} of most highly amplified perturbations as a function of the Reynolds number. (*b*) Ratio $\mathcal{R}_{max}$ of the energy amplification factors of non-parallel and parallel flow as a function of the Reynolds number.

The frequency at which non-modal growth is most effective can be intuitively related to the interaction of the Orr and lift-up mechanisms. The tilting of flow structures by the mean shear in the Orr mechanism requires a finite perturbation length scale and is inactive in the case of zero-frequency perturbations which however maximize the efficiency of the lift-up process. In figure 8(*a*), the frequency of the most highly amplified perturbations is plotted versus *Re*. Larger Reynolds numbers are observed to favour lower perturbation frequencies and thus increase the relevance of lift-up at the expense of the Orr mechanism. With logarithmic scaling for both axes, the relation can be approximated by a straight line, indicating a power law $\omega_{max} \sim Re^{-\zeta}$ with $\zeta \approx 0.8$. An extrapolation of this trend predicts the most highly amplified perturbations to have zero frequency as $Re \to \infty$, consistent with the vanishing of non-parallel effects in the inviscid limit.

Finally, the magnitude of the energy amplification is compared between the parallel and non-parallel cases by evaluating the amplification ratio

$$\mathcal{R}_{max}(x_0) \equiv \max_{\omega} \frac{\max_{x_1} G_{non\text{-}parallel}(x_0, x_1; \omega)}{\max_{x_1} G_{parallel}(x_0, x_1; \omega)}, \tag{3.2}$$

which relates the values obtained for G, maximized over all end points and frequencies at a given x_0 and thus *Re*. The result, presented in figure 8, shows a distinct maximum for $\mathcal{R}_{max}$ near $Re \approx 10^4$ where non-parallel effects extremally enhance algebraic growth through the interaction of Orr and lift-up mechanisms. The result suggests that in the relatively viscous regime at small *Re* where the gain due to algebraic growth is small, non-parallel effects are relatively ineffective at enhancing the amplification of disturbances. The decay at large *Re* is consistent with the aforementioned absence of non-parallel effects in the limit of large Reynolds numbers.

4. Streamwise pressure gradient

Several earlier studies have examined the effect of a streamwise pressure gradient on the non-modal growth of perturbations in boundary layers. Temporal optimal growth analyses in parallel flow by Corbett & Bottaro (2000) showed that adverse pressure gradient (APG) can lead to stronger algebraic amplification. Consistent with parallel analyses of the Blasius boundary layer, their results predicted that the most highly amplified perturbations have zero streamwise wavenumber, independent of

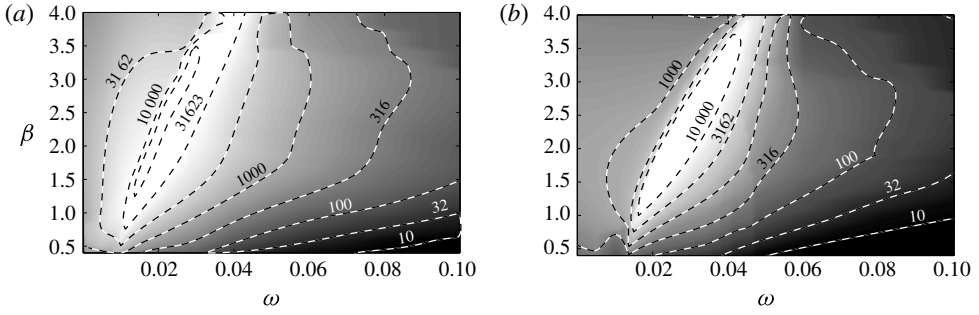

FIGURE 9. Maximum energy amplification ratio G (logarithmic scaling) at $Re_0 = 2440$ as a function of the perturbation frequency ω and the perturbation wavenumber β. (*a*) Adverse pressure gradient. (*b*) Favourable pressure gradient.

the Reynolds number. For short suboptimal time intervals, the most highly amplified disturbances were however characterized by finite streamwise wavenumbers. Linear parallel analyses and nonlinear direct simulations by Zaki & Durbin (2006) led to commensurate results of stronger streaks in the presence of adverse pressure gradient. Stability analyses of streaky boundary layers by Hack & Zaki (2014) showed that adverse pressure gradient can also enhance the secondary instability of streaks, explaining the early breakdown to turbulence observed in APG boundary layers. More recently, Hack & Zaki (2016) demonstrated that the local momentum thickness can act as a similarity parameter across pressure gradients for several attributes of boundary-layer streaks including their amplitude and cross-sectional area.

In the following, we extend the analysis of non-parallel optimal perturbations to boundary layers with streamwise pressure gradient. Both an adverse- and a favourable-pressure-gradient (FPG) case with respective Hartree parameters $H = -0.10$ and $H = 0.10$ are considered. The streamwise and normal base flow is modelled via the Falkner–Skan equations (see e.g. Schlichting & Gersten 2006) with the free-stream velocity following a power law,

$$U(x, y \to \infty) = Cx^m, \tag{4.1}$$

where the constant C was chosen such that $U(x_0, y \to \infty) = 1$. The exponents are $m = -0.0476$ in the APG case and $m = 0.0526$ in the FPG case. It is worth mentioning that the variation of the free-stream convective speed in x, i.e. in the dimension in which the disturbances evolve, is in contrast to temporal analyses, which capture the effect of the pressure gradient only through the (invariable) shape of the base-flow profile. In the following, we scale the amplitudes of the disturbances with $U(x_0, y \to \infty)$. The alternative normalization by the local free-stream speed predicts weaker amplification in the FPG case and higher amplification in the APG case.

The most highly amplified perturbations at Reynolds number $Re_0 = 2440$, corresponding to initial positions $x_0 = 88.1$ (APG) and $x_0 = 137.4$ (FPG), are considered. Analogous to the ZPG flow, the energy gain is again maximized over all possible final positions x_1. Results for G in both flow configurations as a function of the spanwise disturbance wavenumber and the disturbance frequency are presented in figure 9. Adverse gradient enhances the algebraic amplification of disturbances with a global maximum of $G \approx 4.3 \times 10^4$, approximately three times the value found for the ZPG boundary layer. Similar to the Blasius case, the most highly amplified

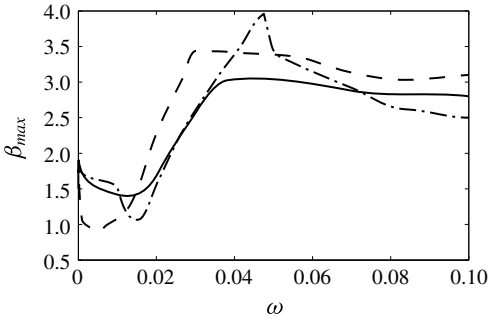

FIGURE 10. Spanwise wavenumber of the most highly amplified perturbations as a function of the perturbation frequency ω at $Re = 2440$. ZPG (black), APG (dashed) and FPG (dash-dotted).

disturbances in both configurations are again found in a limited region of non-zero frequency that is aligned at an angle in the frequency/wavenumber plane. The most energetic perturbations in the APG case are generated at parameters $\beta = 1.8$ and $\omega = 0.01625$. The amplification takes place over the distance $\Delta x = x_1 - x_0 = 41.8$ which is considerably shorter than the distance $\Delta x = 141.8$ of the most highly amplified disturbances in the ZPG case at the same Reynolds number. In line with the existing literature on parallel-flow, comparison with the ZPG case also shows that perturbations with zero frequency are weaker in the FPG case and stronger in the APG boundary layer.

The relation between the scales of the perturbations preferentially generated by algebraic growth is quantified in figure 10. The ordinate indicates the spanwise wavenumber of the most highly amplified disturbances, β_{max}, as a function of their frequency. All three considered flow configurations show linear trends in the region of highest amplification $0.015 \lesssim \omega \lesssim 0.04$. In particular, the slope of the curves is similar in all cases, although shifted to lower frequencies in the adverse pressure gradient.

Visualizations of the most highly amplified disturbances in the APG boundary layer as a function of the phase are presented in figure 11. Similar to the Blasius case, the most energetic perturbations are generated by a combination of the Orr and lift-up mechanisms. At the initial position, the disturbances are tilted to the left at approximately the same angle in the φ–y plane as in the ZPG boundary layer. While the amplification takes place over a shorter distance, the reorientation and thus the angle at x_1 is again comparable to the Blasius case.

5. Conclusions

A method for computing optimal disturbances in spatially developing boundary layers was presented. The scheme is consistent with the assumptions of the parabolized stability equations and circumvents some of the restrictive premises underlying adjoint-based PSE methods. A notable advantage over global analyses is the substantially lower computational cost which allows the effective evaluation of a large parameter space.

Application of the scheme to the parallel ZPG boundary layer yields results that are commensurate with temporal analyses, both in terms of the magnitude of disturbance growth and the associated parameters. In non-parallel flow, additional

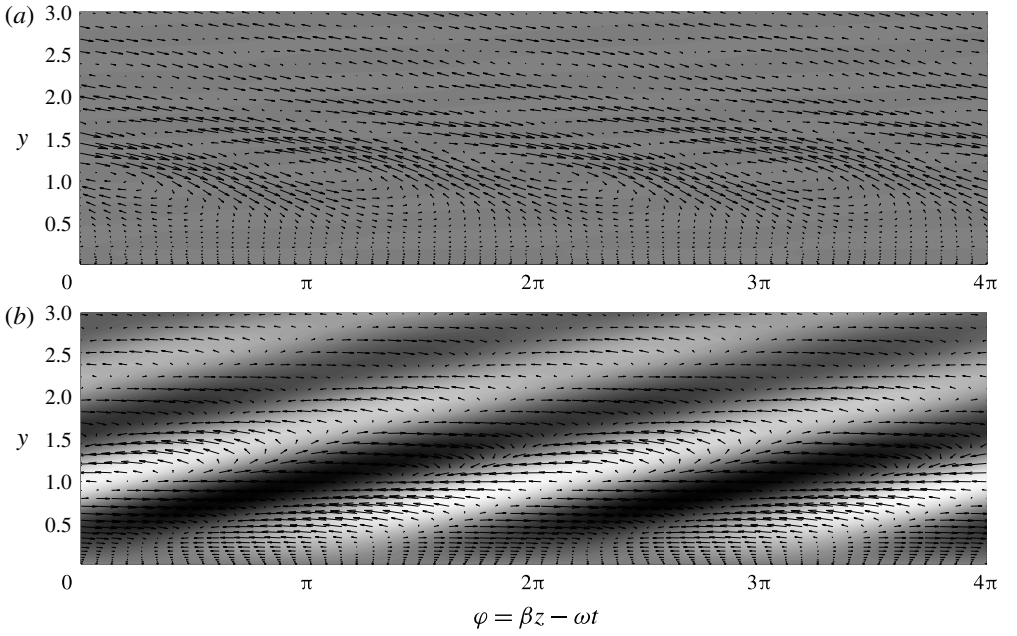

FIGURE 11. Optimal disturbance in APG boundary layer as a function of the phase $\varphi = \beta z - \omega t$. Contours of the streamwise component with vectors of the spanwise and normal components. (*a*) Initial position, $x_0 = 88.1$. (*b*) Position of highest kinetic energy, $x_1 = 129.7$.

growth is observed that is attributed to the combined action of the Orr and lift-up mechanisms. The present results thus substantiate and quantify observations made in global analyses of non-modal disturbance growth which suggested that the most highly amplified perturbations incorporate elements from both mechanisms.

The most energetic disturbances are generated by streamwise vortices that are tilted against the mean shear. The non-parallel effects of boundary-layer expansion and non-zero normal base-flow velocity enhance the efficiency of the Orr mechanism which amplifies perturbations of finite frequency and streamwise extent. At constant Reynolds number, algebraic growth is most effective within a relatively narrow band in the parameter space that is characterized by a linear relation of the disturbance frequency and wavenumber. The additional growth introduced by non-parallel effects is most relevant within a range of moderately high Reynolds numbers and the optimal frequency of the most highly amplified perturbations decreases with Reynolds number. Consistent with the absence of non-parallel effects in the inviscid limit, an extrapolation of the trend predicts that zero-frequency perturbations are most highly amplified in the limit of large Reynolds numbers.

At zero disturbance frequency, the Orr mechanism is rendered inactive as the extended streamwise length scales of the perturbations impede their effective tilting by the mean shear. In this setting, the amplification of perturbations can be entirely ascribed to the lift-up mechanism. The comparable energy gain observed for disturbances with near zero frequency in parallel and non-parallel flow thus suggests that lift-up is only weakly affected by non-parallel effects. By extension, the appreciable sensitivity of algebraic growth to the disturbance frequency may be predominantly attributed to the Orr mechanism.

In formal terms, the added growth in the presence of the non-parallel base flow can be interpreted as the outcome of an increased relevance of non-normal effects. Non-orthogonality enters the initial value problem in parallel flow through the shapes of the individual eigenfunctions and their respective growth rates which however remain constant during the evolution of the disturbances. In the non-parallel base flow, both the shape of the eigenfunctions and their growth rates and wavenumbers vary individually as the disturbances evolve downstream which introduces additional pathways for non-orthogonal effects.

Finally, the influence of a streamwise pressure gradient on the algebraic amplification of disturbances in non-parallel flow was investigated. Moderate favourable pressure gradient led to a modest weakening of algebraic growth compared to the ZPG boundary layer. Owing to the acceleration of the free stream, the resulting perturbations have nonetheless lower relative amplitudes than in Blasius flow. Adverse pressure gradient was shown to appreciably enhance the amplification of disturbances. In all configurations, the disturbance frequency and wavenumber of the most highly amplified disturbances are linked through a linear relation.

Acknowledgements

The authors are grateful to Dr A. Towne for valuable discussions and helpful comments on an earlier version of this manuscript. Support from the Office of Naval Research, the Air Force Office of Scientific Research and Deutsche Forschungsgemeinschaft is acknowledged.

REFERENCES

ÅKERVIK, E., EHRENSTEIN, U., GALLAIRE, F. & HENNINGSON, D. S. 2008 Global two-dimensional stability measures of the flat plate boundary-layer flow. *Eur. J. Mech. (*B*/Fluids)* **27**, 501–513.

ANDERSSON, P., BERGGREN, M. & HENNINGSON, D. S. 1999 Optimal disturbances and bypass transition in boundary layers. *Phys. Fluids* **11** (1), 134–150.

BERTOLOTTI, F. P., HERBERT, T. & SPALART, P. R. 1992 Linear and nonlinear stability of the Blasius boundary layer. *J. Fluid Mech.* **242**, 441–474.

BUTLER, K. M. & FARRELL, B. F. 1992 Three-dimensional optimal perturbations in viscous shear flow. *Phys. Fluids* A **4** (8), 1637–1650.

CORBETT, P. & BOTTARO, A. 2000 Optimal perturbations for boundary layers subject to stream-wise pressure gradient. *Phys. Fluids* **12** (1), 120–130.

FARRELL, B. F. 1987 Developing disturbances in shear. *J. Atmos. Sci.* **44** (16), 2191–2199.

HACK, M. J. P. & ZAKI, T. A. 2014 Streak instabilities in boundary layers beneath free-stream turbulence. *J. Fluid Mech.* **741**, 280–315.

HACK, M. J. P. & ZAKI, T. A. 2015 Modal and nonmodal stability of boundary layers forced by spanwise wall oscillations. *J. Fluid Mech.* **778**, 389–427.

HACK, M. J. P. & ZAKI, T. A. 2016 Data-enabled prediction of streak breakdown in pressure-gradient boundary layers. *J. Fluid Mech.* **801**, 43–64.

HAJ-HARIRI, H. 1994 Characteristics analysis of the parabolized stability equations. *Stud. Appl. Maths* **92**, 41–53.

HERBERT, T. 1994 Parabolized stability equations. In *Special Course in Transition Modelling. AGARD Rep. 793*, pp. 4(1)–4(34).; https://www.sto.nato.int/publications/AGARD/AGARD-R-793/AGARDR793.pdf.

HERBERT, T. 1997 Parabolized stability equations. *Annu. Rev. Fluid Mech.* **29**, 245–283.

JIMENÉZ, J. 2013 How linear is wall-bounded turbulence? *Phys. Fluids* **25**, 110814.

LANDAHL, M. T. 1975 Wave breakdown and turbulence. *SIAM J. Appl. Maths* **28** (4), 735–756.

LANDAHL, M. T. 1980 A note on an algebraic instability of inviscid parallel shear flows. *J. Fluid Mech.* **98**, 243–251.

LI, F. & MALIK, M. R. 1996 On the nature of the PSE approximation. *Theor. Comput. Fluid Dyn.* **8**, 253–273.

LUCHINI, P. 2000 Reynolds-number-independent instability of the boundary layer over a flat surface: optimal perturbations. *J. Fluid Mech.* **404**, 289–309.

MONOKROUSOS, A., ÅKERVIK, E., BRANDT, L. & HENNINGSON, D. S. 2010 Global three-dimensional optimal disturbances in the Blasius boundary-layer flow using time-steppers. *J. Fluid Mech.* **650**, 181–214.

ORR, W. M. F. 1907 The stability or instability of the steady motions of a perfect liquid and of a viscous liquid. Part I: a perfect liquid. Part II: a viscous liquid. *Proc. R. Irish Acad.* **27**, 9–138.

REDDY, S. & HENNINGSON, D. 1993 Energy growth in viscous channel flows. *J. Fluid Mech.* **252**, 209–238.

REDDY, S. C., SCHMID, P. J. & HENNINGSON, D. S. 1993 Pseudospectra of the Orr–Sommerfeld operator. *SIAM J. Appl. Maths* **53** (1), 15–47.

SCHLICHTING, H. & GERSTEN, K. 2006 *Boundary Layer Theory*, 10th edn. Springer.

SCHMID, P. J. 2007 Nonmodal stability theory. *Annu. Rev. Fluid Mech.* **39**, 129–162.

TEMPELMANN, D., HANIFI, A. & HENNINGSON, D. S. 2010 Spatial optimal growth in three-dimensional boundary layers. *J. Fluid Mech.* **646**, 5–37.

TOWNE, A. 2016 Advancements in jet turbulence and noise modeling: accurate one-way solutions and empirical evaluation of the nonlinear forcing of wavepackets. PhD thesis, California Institute of Technology.

TREFETHEN, L. N., TREFETHEN, A. N., REDDY, S. C. & DRISCOLL, T. A. 1993 Hydrodynamic stability without eigenvalues. *Science* **261** (5121), 578–584.

ZAKI, T. A. & DURBIN, P. A. 2006 Continuous mode transition and the effects of pressure gradients. *J. Fluid Mech.* **563**, 357–358.